Journal of Materials Science & Technology 34 (2018) 2140–2148

Contents lists available at ScienceDirect

Journal of Materials Science & Technology

journal homepage: www.jmst.org

Interaction between austein-ferrite phases on passive performance of 2205 duplex stainless steel

Xuequn Cheng[a,*], Yi Wang[b], Xiaogang Li[a,*], Chaofang Dong[a]

[a] Institute of Advanced Materials and Technology, University of Science and Technology Beijing, Beijing 100083, China
[b] Mechanical and Aerospace Engineering Department, West Virginia University, Morgantown, WV 26506, USA

ARTICLE INFO

Article history:
Received 27 November 2017
Received in revised form
21 December 2017
Accepted 1 January 2018
Available online 13 February 2018

Keywords:
Duplex stainless steel
Phases
Passivation
Semiconductor
Corrosion

ABSTRACT

The passive behavior of 2205 duplex stainless steel (DSS) and its individual phases (α-phase, γ-phase) in neutral 3.5% NaCl solution was investigated by various electrochemical methods. The results indicated that galvanic effect between α and γ phases cannot deteriorate local corrosion, but favors the enhancement of the passive film. Under the galvanic effect, the diffusion of the dissolved passive cations would be promoted in a short distance between α and γ zones, leading to modifications of the chemical composition and semiconductive property of the passive film and therefore the enhancement of the corrosion resistance of DSS 2205.

1. Introduction

Duplex stainless steels (DSSs), known as a two-phase structure comprising island-like austenite (γ-phase, fcc) and continuous ferrite matrix (α-phase, bcc) [1–4], possess excellent mechanical properties and high corrosion resistance, and thus are widely employed in various industrial fields, such as oil, chemical, petroleum (offshore), and electric power industries. The passive film on stainless steels, which is a key to the high corrosion resistance, is strongly influenced by alloy elements. Therefore, a heterogeneous passive film is formed on DSS, due to the different chemical compositions of two constituent phases. Especially, Cr and Mo are more enriched in α-phase, while Ni and Mn are more partitioned in γ-phase [5–7]. Thus, the passive behavior of each phase of DSS is important, because the weaker phase shows the dominant effect on the overall corrosion behavior. Additionally, the interaction effect of these two phases of DSS on the whole passive performance is also worth of discussing, since DSS exhibits greater corrosion resistance than conventional single-phase stainless steels, such as ferrite and austenitic stainless steels, in chloride-rich media [8,9].

With the widespread use of DSSs in more aggressive environments, more detailed information about the passive film on single-phase and dual-phase is definitely needed. However, there are still several important aspects about the essential reason for the higher corrosion resistance of DSSs than single-phase stainless steels, which are not fully understood. Olsson [10] studied the passivity of single phase of DSS by using alloys with compositions similar to austenite and ferrite phases, indicating that the anti-corrosion ability could be partially owed to the interaction between the austenite and the ferrite. But the exact element contents of the composed phases of DSS were not ascertained in this work, and thus the passive properties of single-phase cannot be precisely presented.

Fortunately, selective dissolution technique, as a novel preparation of single-phase samples, was proposed by Tsai et al. [11,12]. According to those reports, for 2205 DSS as reported in mixed H_2SO_4/HCl solution, two anodic peaks existed in the active-to-passive transition region of the potentiodynamic polarization curves: one for selective dissolution of γ-phase (−255 mV vs saturated calomel electrode, SCE) and the other for α-phase (−320 mV vs SCE). After etching DSS samples at the two characteristic potentials for 10 h, exclusive γ-phase and α-phase could be exposed, respectively. Thus, the single-phase electrodes could show exact chemical compositions as the counterparts of DSS. Using this etching technique, it has been revealed that the coupling effect of the constituent phases in DSS enhanced the stability of Cr^{3+} species in

* Corresponding authors.
E-mail addresses: chengxuequn@ustb.edu.cn (X. Cheng), lixiaogang@ustb.edu.cn (X. Li).

https://doi.org/10.1016/j.jmst.2018.02.020
1005-0302/

the passive layer and thus benefited the overall passive behavior [13].

Moreover, localized electrochemical measurements, including localized electrochemical impedance spectroscopy (LEIS) and scanning vibrating electrode technique (SVET), are massively employed in corrosion science in the past decade [14,15]. Compared to traditional electrochemical techniques, these new methods could be employed for in situ tests and mechanism research more conveniently, due to the capability of obtaining local electrochemical signals at the micrometer scale. The local electrochemical reactions that occurred in an iron-zinc galvanic couple immersed in aqueous sodium chloride solution has been revealed by SVET and scanning electrochemical microscope (SECM) techniques [16]. Cheng et al. [17] also studied the local galvanic corrosion between coupled TA2 and 316L stainless steel by these techniques. For DSS, the constituent phases are always at micrometer magnitude, and thus these techniques are well suited to characterize the passivity and coupling effect.

In the present work, single α and γ phase would be fabricated from 2205 DSS samples by selective dissolution. Their passive behavior and interaction were investigated by comparing with the dual-phase electrode (2205 DSS) in 3.5 wt% NaCl solution. Various electrochemical methods, such as OCP (open circuit potential), potentiodynamic curves, EIS (electrochemical impedance spectroscopy) and Mott-Schottky plots, were employed in the study. XPS (X-ray photoelectron spectrometer) and SEM (scanning electron microscopy) together with EDS (energy dispersive spectroscopy) were also used for compositional analysis. LEIS and SVET were applied to characterize the coupling effect between the constituent phases. It is anticipated that the result provides an essential insight to the passive behavior of single phase of 2205 DSS and the interaction between both phases on the electrochemical behavior of the material.

2. Experimental

2.1. Sample preparation

The composition (wt%) of the sample is as follows: Si 0.59, Mn 1.2, P 0.029, Mo 2.62, Cr 22.57, Ni 4.63, C 0.029, S 0.0043, N 0.13, and Fe balance. The 2205 DSS steel sheet with thickness of 5 cm was solution heat treated at 1100 °C for 30 min, and then water quenched. The samples were prepared with size of 10 mm × 10 mm, welded to wires, embedded in epoxy resin leaving a working area of 1 cm^2. The sample surface was ground with 400–2000# SiC papers and then rinsed in distilled water, ethanol and acetone.

2.2. Selective dissolution

The solution for selective dissolution was a mixed 2 M H_2SO_4 + 0.5 M HCl. A VMP3 advanced electrochemical system from Princeton Applied Research was used to perform the electrochemical experiment.

A saturated calomel electrode (SCE) was served as the reference electrode and a platinum foil was employed as the counter electrode. The characteristic peak potentials, −255 mV vs SCE and −320 mV vs SCE, were selected for potentiostatic etching of 10 h to ensure the selective dissolution in the specified phase, leaving almost exclusive α-phase or γ-phase exposed on the surface, respectively. After potentiostatic etching, specimens were observed by SEM and EDS.

The preparation process of single-phase electrode is as follows: firstly, the etched sample surface was filled with epoxy resin and put into a vacuum chamber. With the increase of vacuum degree, jammed air in the cavities caused by selective dissolution expelled and epoxy resin filled in. Lasting for 24 h, the epoxy resin was then carefully removed with 2000# SiC papers and then polished, leaving almost exclusive phase exposed on the surface. After the sequences for single-phase electrode preparation, specimens exposed exclusive phase on the surface, were composed of α-phase when 2205 DSS etched at −255 mV vs SCE and γ-phase when etched at −320 mV vs SCE according to the document [11]. These prepared single-phase electrodes and dual-phase sample with an exposed area 1 cm^2 were used for subsequent electrochemical tests. The real surface areas of single-phase samples were obtained by the image analysis.

2.3. Electrochemical tests

The electrochemical behavior of α-phase and γ-phase and dual-phase electrodes were investigated in 3.5 wt% NaCl solution at ambient temperature (25 °C) with electrochemical testing device as mentioned above. The working electrodes were initially reduced potentiostatically at −1.0 V vs SCE for 20 min to remove air-formed oxides, and then OCP curves were recorded for 30 min. EIS tests were obtained with the frequency from 100 kHz to 10 mHz. 10 mV was chosen as the peak to peak amplitude. To interpret the EIS data on the basis of equivalent electric circuits, ZSimpWin software was used. Moreover, the potentiodynamic polarization tests were carried out at a potential scan rate of 0.1667 mV/s from −0.6 V vs SCE until anodic current density reached 1 mA/cm^2. Measurements of capacitance were performed on films of specimens with the frequency of 1 kHz from −0.6 V vs SCE to 1.0 V vs SCE. Similarly, the peak to peak amplitude single was 10 mV, and the scan rate was 45 mV/s. Sufficient short testing time ensured the stability of passive films during the test while the capacitance was measured as a function of potential.

The localized electrochemical measurements were performed through a PAR Model 370 scanning electrochemical workstation, which was composed of a 370 scanning control unit, a M236A potentiostat, a M5210 lock-in amplifier, and a video camera system. The 3.5 wt% NaCl solution was used as test solution. A single-phase α sample and a single-phase γ sample were prepared by the selective dissolution technique. They were electrical connected and fixed by epoxy resin. Then the cured resin on the selective dissolved surface was carefully removed with 2000# SiC papers and polished, exposing α single-phase on one side and γ single-phase on the other side. The two-phase-coupled specimen working electrode is represented in Fig. 1. An SCE was employed as reference electrode and a platinum plate as counter electrode. Area-scan mode was used in LEIS measurements. The platinum microprobe with a 10 μm tip was set above the working surface. The measurement frequency was fixed at 10 Hz with applied AC amplitude of 10 mV at open circuit potential.

$$i = -\frac{k\nabla\phi}{d} = -\frac{\nabla\phi}{\rho d}$$

where i is the localized current density of specimen, ∇F is the potential gradient over the test area in the solution, κ is the conductivity of the solution, ρ is the resistivity of the solution and d is the amplitude of the platinum tip microprobe.

In 3.5 wt% NaCl solution, anodic process is characterized by the dissolution of iron:

$$Fe \rightarrow Fe^{2+} + 2e^- \quad (1)$$

Cathodic process is characterized by the reduction of dissolved oxygen:

$$O_2 + 2H_2O + 4e^- \rightarrow 4OH^- \quad (2)$$

Reaction (1), which leads to an upward flow of metal cations above the test region, is detected as negative currents. Conversely,

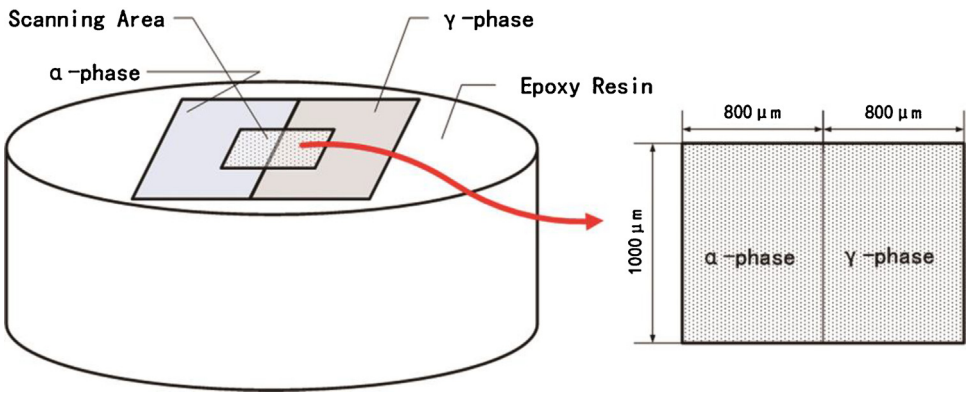

Fig 1. Schematic diagrams of two-phase-coupled specimen for LEIS and SVME measurements.

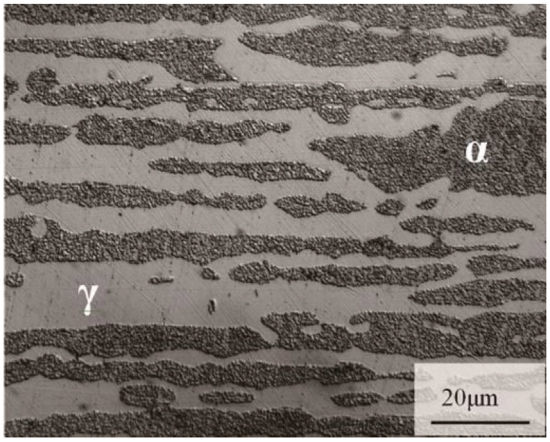

Fig. 2. Optical micrograph of 2205 DSS after solution heat treated at 1100 °C for 30 min followed by water quenching, the dark phase is α-phase while white region is γ-phase. Image analysis shows the volume ratio of α/γ is 56/44.

reaction (2) is detected as positive currents. With the presence of passive film, the currents on the test area are hard to be detected at open circuit potential. A constant current of −10 μA was applied on the specimen by galvanostat to strengthen the signal.

2.4. XPS surface analysis

The chemical composition of air-formed oxide films on α-phase, γ-phase and dual-phase was investigated by XPS. XPS experiments were excited by monochromatic Al K_α radiation source operated at 150 W. The XPS curve fitting was performed by the commercial software Xpspeak version 4.1, which contained the Shirley background subtraction and Gaussian-Lorentzian tail function for a better spectra fitting.

3. Results and discussion

3.1. Morphology and chemical composition of single-phase

It is generally known that the alloy content and microstructure play an important role in corrosion resistance of steel. The micrograph of 2205 DSS after solution heat treatment at 1100 °C for 30 min is examined by optical microscopy (Fig. 2). Etched by aqua-regia reagent, dark region of microstructure is ferrite (α-phase), while white region is austenite (γ-phase), and the surface area ratio of α/γ is about 56/44.

Fig. 3 shows the SEM and MFM morphologies of the samples after potentiostatic etching. As shown in Fig. 3(a), α-phase is exposed on the surface after etching at potential of −255 mV vs SCE for 10 h, and Fig. 3(b) reveals γ-phase when etching at −320 mV vs SCE according to the document [11]. The MFM morphologies of two single-phase samples are presented in Fig. 3(c) and (d). It is evident that the only phase exposed on the surface of γ-phase and α-phase samples is paramagnetic γ-phase and ferromagnetic α-phase, respectively, while the cavities are filled with epoxy resin. Therefore, it can be claimed that single-phase samples are well prepared.

Table 1
EDS results of the major alloying elements (wt%) of 2205 DSS etched at the potential of −255 mV and −320 mV.

Etching potential	Si	Cr	Ni	Mo	Mn	Phase
matrix	0.59	22.57	4.63	2.62	1.2	Dual
−255 mV	0.77	24.67	3.79	3.81	1.49	α
−320 mV	0.56	21.36	6.93	2.76	1.72	γ

It is obviously seen that potentiostatic etching can lead to selective dissolution of specific phase, leaving another phase almost not affected and resulting in the formation of cavities and convex. In order to identify the compositions of single α-phase and γ-phase, EDS serves to analyze the major alloying elements, such as Fe, Cr, Mo, Ni and Mn. The elements concentrations of phase almost unaffected taken at least ten points averaged are listed in Table 1. It can be seen that the amount of Si, Cr and Mo was more in α-phase than that in γ-phase, while the amount of Ni was vice versa. Similarly, it can be demonstrated again that the surface area ratio of α/γ is about 56/44.

3.2. Interaction of α/γ phases on the electrochemical behavior of 2205 DSS

Due to the surface area ratio of α/γ (56/44), the real measured areas of α- and γ-phase electrodes are 0.56 and 0.44 cm^2, respectively. Fig. 4 shows the quasi-steady polarization curves of dual-phase, γ-phase and α-phase electrodes in 3.5 wt% NaCl solution, marked with three different passive zones. The dual-phase and γ-phase samples begin to passivate at similar potential while α-phase starts to be passive at more positive potential, and the breakdown potentials (E_b) of the three samples are nearly identical (E_b = 1.02 V_{SCE}). In fact, according to the Pourbaix diagram for water, when the potential reaches about 1 V, the oxygen evolution occurs, which is indicated by the following specific relationship (3),

$$E_e = 1.229 + 0.0148 \lg P_{O2} - 0.0591\ pH \quad (3)$$

where E_e is the equilibrium potential of the oxygen electrode, P_{O2} is the partial pressure of oxygen. Therefore, these identical breakdown potentials are not really the pitting potentials, but the

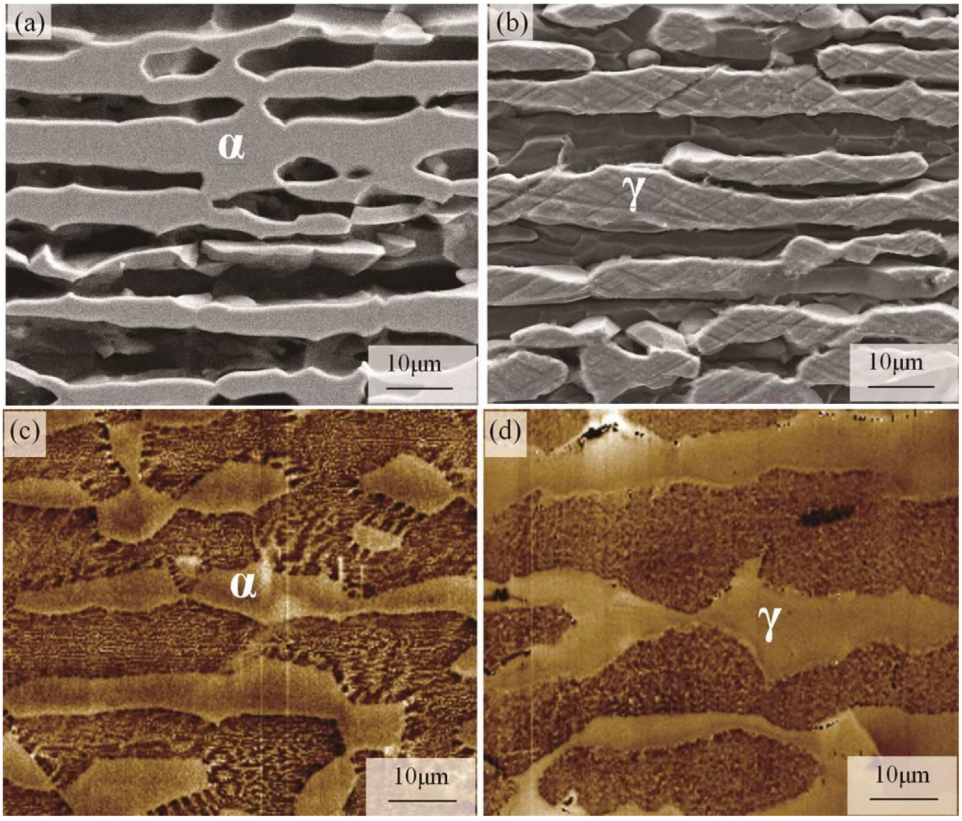

Fig. 3. SEM morphologies of (a) α-phase etched at −255 mV for 10 h, (b) γ-phase etched at −320 mV for 10 h; and MFM morphologies of (c) α-phase (d) γ-phase; both samples were well fabricated after the single-phase preparation procedures.

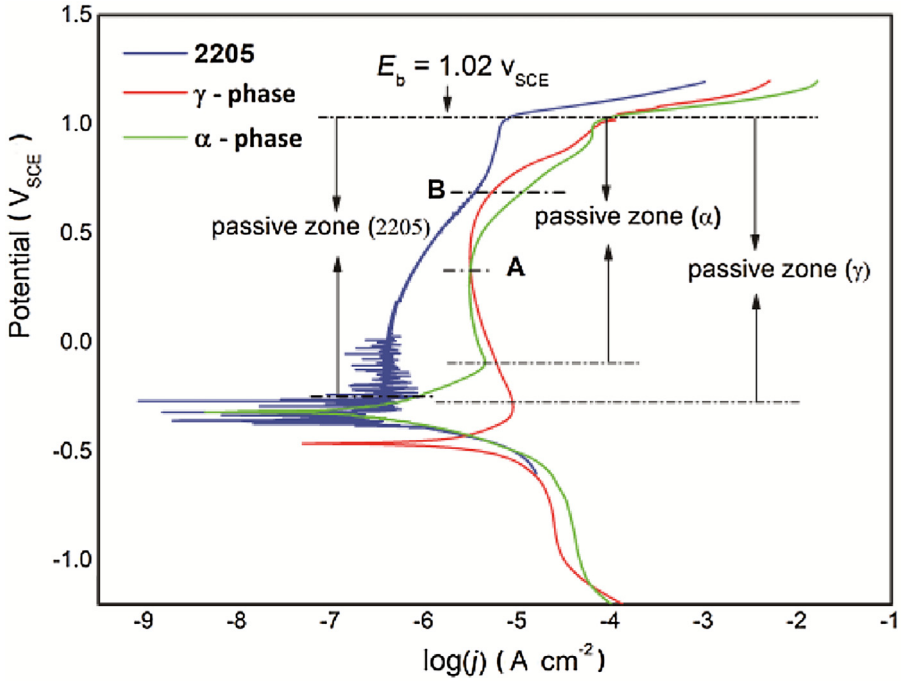

Fig. 4. Potentiodynamic polarization curves of α-phase, γ-phase and dual-phase specimens in 3.5 wt% NaCl solution.

potentials under which oxygen evolution occurs. The result indicates that DSS and γ-phase samples are more inclined to passivate than α-phase.

Passive current density (i_p) is a key parameter to assess the properties of passive films. Although there is no distinct difference between the passive current density of γ-phase (i_p^{γ}) and α-phase (i_p^{α}), i_p^{γ} is clearly lower than i_p^{α} in the relatively higher potential region ($E > E_A$), revealing that γ-phase's passive film is more stable than α-phase. However, the passive current density of 2205 DSS sample (i_p^{2205}) is much more lower about one order of mag-

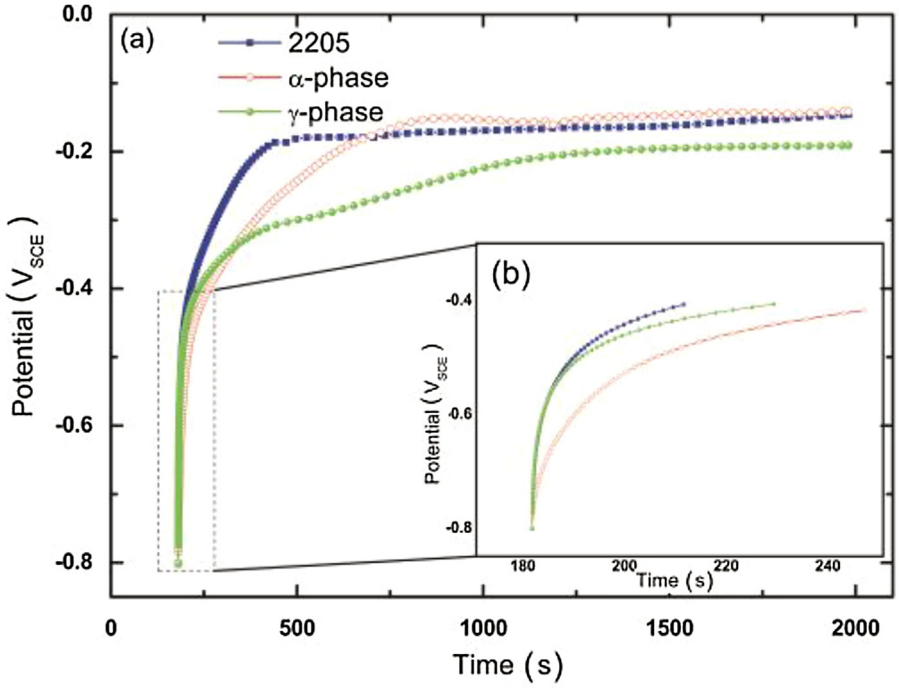

Fig. 5. OCPs curves of α-phase, γ-phase and dual-phase specimens in 3.5 wt% NaCl solution for 1800s.

nitude than i_p^{γ} and i_p^{α} in the whole passive zone. When $E_b > E > E_B$ ($E_B = 0.69\ V_{SCE,}$ indicated in Fig. 4), i_p^{2205} remains the lowest value, while i_p^{γ} and i_p^{α} begin to grow rapidly. When the potential reaches E_b, i_p^{2205} is still lower over one order of magnitude than i_p^{γ} and i_p^{α}, even though E_b of the three samples are nearly identical. It indicates that the chemical stability of the passive film on dual-phase sample is much better than that of the other single-phase samples. That is, the interaction of α and γ in 2205 DSS is liable to form chemically stabler film.

Fig. 5(a) shows the OCP curves of the three specimens in 3.5 wt% NaCl solution for 1800s. It can be seen that the potentials increase rapidly at the beginning, and then reach a steady value.The OCP values of dual-phase and γ-phase samples are similar, but higher than that of α-phase sample. Fig. 5(b) is the complement of Fig. 5(a), which shows the potential increase rate of the three samples at the first 240 s of the OCP tests. Generally, the slope change of OCP curves is related to the growth process of passive film. Initially, the potential increase rate of α-phase is higher than that of γ-phase (Fig. 5(b)), which is due to the higher content of Cr in α-phase because Cr could benefit the re-passivation performance [18,19]. But later (the time interval from 240 s to the steady sate), the potential increase rate of γ-phase is beyond that of α-phase, which could be attributed to the beneficial effect of Ni [20,21]. At these two regions, 2205 DSS sample possesses the highest potential increase rate, which shows a good accordance with the results of quasi-steady polarization tests. In other word, the interaction of α and γ in 2205 DSS favors the formation of passive film.

EIS is employed to characterize the properties of the passive film. Firstly, Kramers-Kronig transform is used to validate the EIS test for the electrochemical system [22–24]. The testing system is stable and thus the data is reasonable. Fig. 6(a) is the result of Kramers-Kronig transform on the Bode plots of three samples in 3.5% NaCl solution with the immersion time of 12 h under OCP condition, indicating that the testing system is stable and the obtained EIS data are valid. It is clearly seen that the Bode plots of all the three specimens display 2 time constants, corresponding to 2 different main electrode reactions during passivation. It can also be seen that |Z| value of 2205 sample is markedly higher than that of the two single-phase samples, while these single-phase samples show similar responses to frequency signals. It indicates that the main reactions of γ-phase and α-phase electrodes under the passive state would be similar, which are commonly recognized as the charge transfer process of the double layer and passivation process within the passive film [25]. But their combination, that is, the interaction of α and γ will greatly influence the passivation process and the property of passive film. Fig. 6(b) is the Nyquist plots of the three samples. In agreement with the results in Fig. 6(a), the plots of two single-phase specimens are similar and both show significant difference with that of dual-phase sample.

Different electrical equivalent circuit (EEC) models have been used for the interpretation of EIS plots on stainless steel surface [4,5,26,27]. In the present work, the EEC shown in Fig. 6(b) is chosen to fit the experimental data because the three samples do not undergo pitting corrosion and thus possess intact passive films, with solution resistance R_s, charge transfer resistance of the double layer R_t or outer passive layer resistance R_{outer} in parallel with the related constant phase element CPE_1, passive layer assistance R_p and inner passive layer resistance R_{inner} in parallel with the related CPE_2 [28,29]. CPE is widely used to replace the pure capacitance element C to reflect the capacitance behavior in terms of the dispersion effect. Its admittance Y is given by the following equation [30,31]:

$$Y = Y_0(jw)^n, \tag{4}$$

where w is the angular frequency (rad s^{-1}), Y_0 is the constant representative for the CPE (Ω^{-1} cm^{-2} s^n), $j^2 = -1$, the CPE power n, is an adjustable fit parameter that lies between 0 and 1. CPE expresses as resistance when $n = 0$, capacitance when $n = 1$, and when $n = 0.5$ the CPE represents a Warburg impedance. The key parameters obtained from the fitting are given in Table 2.

As shown in Table 2, the values of n_1 for γ-phase and α-phase are around 0.5, meaning that the reaction corresponded to the middle-frequency time constant (R_t and CPE_1) has the property of diffusion and thus would happen in the double layer. Meanwhile, due to the

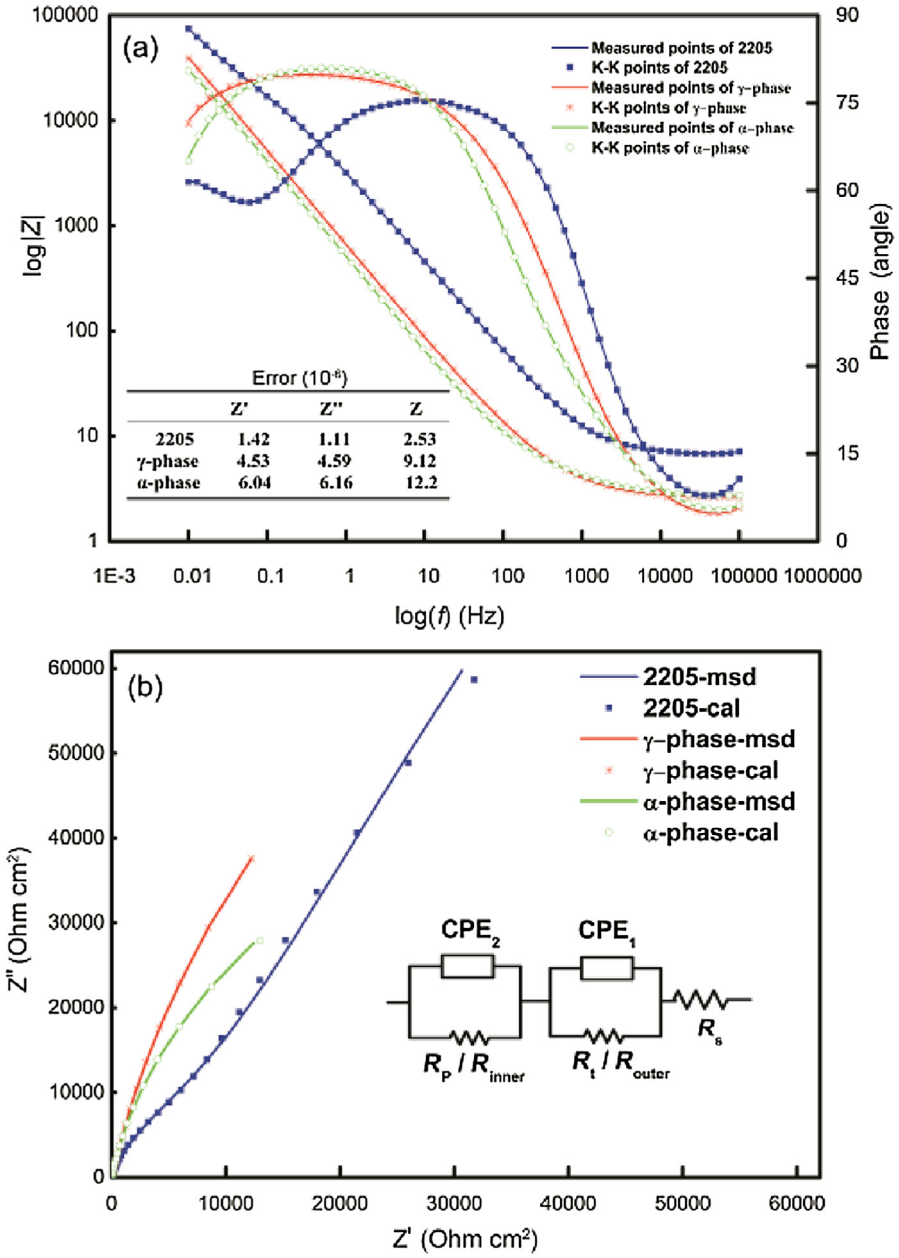

Fig. 6. Nyquist plots of α-phase, γ-phase and dual-phase specimens in 3.5 wt% NaCl solution after 1800s stabilization at open-circuit potential.

Table 2
Key parameters for the impedance spectra obtained in 3.5 wt% NaCl solution after 12 h stabilization at open-circuit potential.

	R_s (Ω cm^{-2})	Y_1 (Ω^{-1} cm^{-2} s^n)	n_1	R_t/R_{outer} (Ω cm^{-2})	Y_2 (Ω^{-1} cm^{-2} s^n)	n_2	R_p/R_{inner} (Ω cm^{-2})
α-phase	2.54	5.24 E-3	0.53	5.1	3.67E-4	0.91	1.06 E5
γ-phase	2.47	1.31 E-2	0.48	10.7	2.91 E-4	0.90	2.61 E5
dual-phase	6.47	1.74 E-4	0.94	4769	1.34 E-4	0.80	5.39 E5

huge values of R_p for γ-phase and α-phase, it is obvious that the low-frequency time constant (R_p and CPE_2) is related to passivation process. However, because the n_1 value of 2205 sample is around 0.94 and R_{outer} value is much larger than R_t, the time constant (R_{outer} and CPE_1) should not be associated with the reaction occurring in the double layer, but the passive process in the outer layer of the passive film. In addition, although the middle-frequency time constant in the EIS plots of 2205 sample is attributed to the reaction in the outer part of the passive film, it does not mean that the charge transfer process in the double layer does not happen, but just that the much smaller signal of charge transfer process was covered by the response of passive process in the outer layer of the passive film. Moreover, it is clearly seen that the passive ability of 2205 DSS sample is greatly better than each of the single phases by comparing the values of R_p and R_{inner}. The passive film of γ-phase is more stable than that of α-phase, which is in agreement with the results discussed above.

In order to further ascertain the interaction between α and γ on the passive behavior, LEIS measurement was performed on the sample prepared as Fig. 1. Fig. 7 shows the result of the LEIS mea-

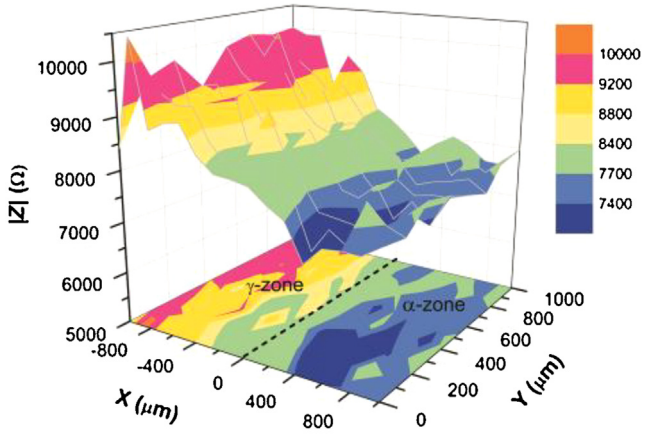

Fig. 7. LEIS result of the two-phase-coupled specimen in 3.5 wt% NaCl solution.

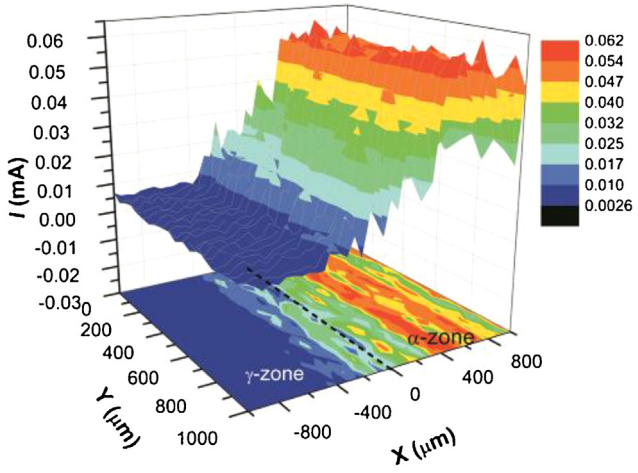

Fig. 8. SVME result of the two-phase-coupled specimen in 3.5 wt% NaCl solution.

surement. It can be seen that there exists two impendence value (|*Z*|) terraces far from the borderline between α and γ phases. The higher |*Z*| terrace, which corresponds to γ phase, is about 9000–10000 Ω, while the lower |*Z*| terrace, which corresponds to α phase, is just about 7500 Ω. The higher the |*Z*| is, the better the corrosion resistance of the passive film is, indicating that the passive film of γ-phase is more corrosion resistant than that of α-phase. Moreover, a distinguishing transition region with a width of 700 μm can be observed near the borderline, which decreases from the γ-phase zone to α-phase. On the base of our previous results, it is anticipated that a |*Z*| peak would appear around the borderline, which would correspond to the interaction of α/γ. Or, there would be a minimum value between the two |*Z*| terraces, similar to the result of the document [32], which investigated galvanic coupling between carbon steel and zinc by LEIS and found a minimum in the vicinity of the interfacial zone because of the strong galvanic effect. However, both cases did not occur. A further SVME measurement on such sample also presents the same phenomenon (Fig. 8).

The above results indicate that there exists appreciable electrochemical difference between α and γ, and then galvanic effect will occur near their interface. However, the case similar to the document [32] did not occur, indicating that the galvanic effect would not cause the local deterioration of the more active α phase. In virtually the galvanic effect enhances the passive film on α phase (The |*Z*| increases and the *I* decrease on the α side near the borderline). That no |*Z*| peak is observed can be attributed to the sphere of the galvanic effect. When α and γ are macro-scale connected (just like

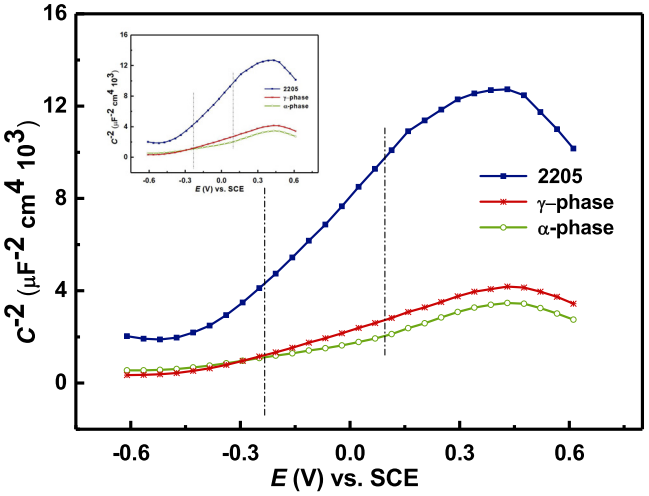

Fig. 9. Mott-Schottky approach for films formed on α-phase, γ-phase and dual-phase specimens in 3.5 wt% NaCl solution.

this work), the interaction of α/γ disperses. While α and γ phases distribute lamellarly and finely (like DSS 2205), the interaction of α/γ would be appreciable. The mechanism may be similar to the document [33]. Under the galvanic effect, the diffusion of the dissolved Ni, Cr or Mo cations would be promoted in a short distance between α and γ zones, leading to the stability enhancement of the passive film. This indicates that the further fined α and γ phases would markedly enhance the passive film on DSS 2205. Such work is going on in our lab.

3.3. Interaction of α/γ phases on the passive film

The significant electrochemical behavior for 2205 DSS by the interaction of α/γ phases can be attributed to the distinct semiconductor property and microstructure of the passive film. The semiconductor properties on the passive film of stainless steels are always investigated by capacitance measurements. And it is common to assume that the measured capacitance of the metal-electrolyte interface can be described by the equation shown as below,

$$\frac{1}{C} = \frac{1}{C_{SC}} + \frac{1}{C_H}, \tag{5}$$

where C_{SC} is the space charge layer capacitance of passive film, and C_H is the Helmholtz capacitance. In general, the capacitance of the space charge layer is much smaller than that of Helmholtz layer and thus the contribution of the Helmholtz capacitance could be neglected when the potential are applied with a sufficiently high frequency. Mott-Schottky approach is based on the Mott-Schottky relation, which describes the potential dependence on the space charge capacity, *C*, when a semiconductor electrode is under depletion condition

$$\frac{1}{C^2} = \pm\frac{2}{eN\varepsilon\varepsilon_0 A^2}\left(E - E_{FB} - \frac{kT}{e}\right), \tag{6}$$

where the positive sign is for n-type and the negative sign for p-type conductivity, *N* is charge carrier density, N_D and N_A represent the donor or acceptor density, *e* is the electron charge, ε is the relative dielectric constant of the semiconductor, 15.6 as in the literature, ε_0 is the vacuum permittivity with the value of 8.85×10^{-14} F/cm, *k* is the Boltzmann constant (1.38×10^{-23} J/K), *T* is the absolute temperature, *E* is the applied electrode potential and E_{FB} is the flat-band potential.

Fig. 9 shows the Mott-Schottky curves in the potential range from −0.5 to 0.4 V for the samples, in which a linear relationship

Table 3
Calculated values of N_D and E_{FB} of films formed on α-phase, γ-phase and dual-phase.

	N_D (10^{20} cm^{-3})	E_{FB} (V_{SCE})	R^2 (%)
α-phase	25.9	−0.569	97.8
γ-phase	19.3	−0.515	99.8
dual-phase	6.2	−0.570	98.9

can be observed and an n-type semiconductor behavior for all three samples' passive films can be determined. The calculated values of donor densities (N_D, which can be an indicator of the density of point defect in the passive film) and flat-band potential (E_{FB}) according to Eq. (4) are listed in Table 3.

Obviously, the N_D values are ranked as dual-phase sample < γ-phase < α-phase. According to point defect model (PDM) [34–36], N_D can be an indicator of cation vacancy density originated from dissolving of cations at the interface of passive film/solution, whose magnitude and migration determine the growth and breakdown of the passive layer. Therefore, the lower N_D value indicates the lower dissolving rate of the cations at the interface of passive film/solution, that is, the better the chemical stability of the passive film. Therefore, the chemical stabilities of the films on these three samples are in the order as follows: dual-phase sample > γ-phase > α-phase. Apparently, the interaction of α/γ phases decreases the dissolving rate of cations in the film and enhances the chemical stability of the passive film.

Fig. 10 displays the detailed spectra of O 1s, Fe $2p_{3/2}$ and Cr $2p_{3/2}$ in the oxide films formed on α-phase, γ-phase and dual-phase samples. After background substraction according to Shirley [37], the XPS results are separated into contributions to the different oxidation states by a fitting procedure. The possible states in passive films can be marked by means of the standard peak spectra from Handbook of X-ray photoelectron spectroscopy [38], as shown in Table 4.

Table 4
Binding energies E_{be} of XPS-peaks of standards.

Fe $2p_{3/2}$	Peak	Fe(0)	Fe_3O_4	FeO	Fe_2O_3	FeOOH
	E_{be}/eV	707.7	708.2	709.4	710.9	711.8
Cr $2p_{3/2}$	Peak	Cr(0)	Cr_2O_3	$Cr(OH)_3$	CrO_3	
	E_{be}/eV	574.3	576.8	577.3	578.3	
O 1s	Peak	O^{2-}	OH^-			
	E_{be}/eV	530.2	531.5			

From the fitting of signals in Fig. 10(a), (d), (g), it can be seen that there exist peaks at about 530.4 eV and 530.7 eV in spectra of O1s, which can be assigned to OH^- and O^{2-} species. OH^- is the primary constituent of the films formed in the air, which relates to the formation of $Cr(OH)_3$ and FeOOH while O^{2-} is the primary constituent of Cr_2O_3, Fe_2O_3 and FeO. Meanwhile, it is also worth noting that there is a relatively higher content of OH^- specie was observed in films formed at γ-phase. From Fig. 10(b), (e), (h), peaks at about 706.9 eV, 708.0 eV, 709.2 eV, 711.0 eV, and 712.0 eV exist in the spectra, which can be assigned to Fe(met), Fe_3O_4, FeO, Fe_2O_3 and FeOOH species. Fig. 10(c), (f), (i) represents the chromium pro-

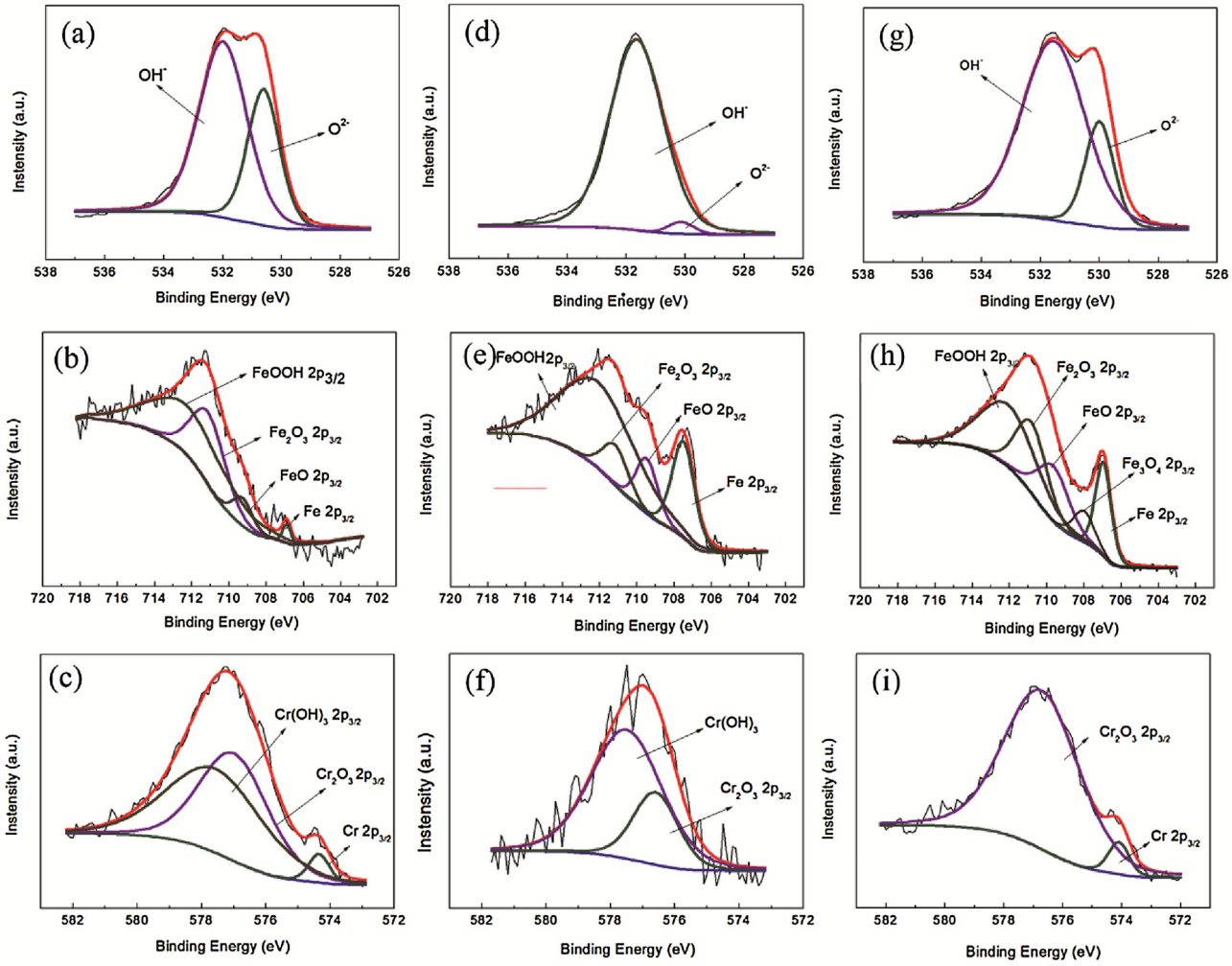

Fig. 10. Detailed XPS spectra of O 1s, Fe $2p_{3/2}$ and Cr $2p_{3/2}$ in air-formed films on α-phase, γ-phase and dual-phase specimens. (a)–(c) For α-phase, (d)–(f) for γ-phase and (g)–(i) for dual-phase specimens.

Table 5
Contents of Cr and its compounds of passive film formed on 2205 DSS determined from XPS.

	α-phase	γ-phase	Dual-phase
Cr (wt%)	3.75	–	5.41
Cr_2O_3 (wt%)	46.18	31.86	94.59
$Cr(OH)_3$ (wt%)	50.07	68.14	–

file in passive films on specimens. The Cr $2p_{3/2}$ spectra in film formed on γ-phase shows mainly two peaks, the peaks around 577.5 eV is attributed to $Cr(OH)_3$, and peak at 576.9 eV is due to Cr_2O_3, respectively. Similarly, the film formed on α-phase reveals the presence of Cr_2O_3, and $Cr(OH)_3$, respectively. The contents of Cr and its compounds determined from XPS are listed in Table 5.

The films on two single phases have similar chemical composition, corresponding to their corrosion resistance. And yet, it is worth noting that the $Cr(OH)_3$ is not detected in film formed at 2205 DSS, Cr_2O_3 maybe the single species and the intensity of the Cr_2O_3 states are apparently higher than those formed at α-phase or γ-phase, and the content of Cr_2O_3 in passive film of α-phase was higher than that of γ-phase.

Generally, chromium in the oxide layer plays important roles in electronic properties and corrosion resistance of films. A heterogeneous passive film was formed on duplex stainless steel due to the differences in chemical composition between γ-phase and α-phase [39]. From the published document [40], Cr_2O_3 is an intermediate oxide, which is the most stable solid chromium and has the properties between network forming (Cr—O—Cr) and modifying oxide, compared with the hydroxides $Cr(OH)_2$, $Cr(OH)_3$, and the oxides CrO_2, and CrO_3. And an increase of hydroxides in the passive film also exhibited harmful effects on the corrosion resistance of stainless steel [41–43]. Therefore, it is the critical factor to the chemical stability of passive film. And the passive film would possess different N_D. In extreme situation when potential reaches transpassive region most Cr^{3+} is incorporated as Cr^{6+} in the passive film and the oxycompound dissolves faster in acidic solutions [44,45].

The current result indicates that the interaction between α and γ increases the amount of Cr_2O_3 in the passive film, leading to the decrease of the dissolved cations from the passive film, that is, leading to the decrease of N_D. With the modification of chemical composition and semiconduct property of the passive film, the corrosion resistance of 2205 DSS is appreciably enhanced comparing with the single phases. Although there exists potential difference between γ-phase and α-phase, galvanic effect between α and γ phases cannot deteriorate local corrosion, and it may promote the diffusion of the passive cations in short distance and be beneficial to the passive behavior of 2205 duplex stainless steel [46]. Some indirect evidences have been reported that acicular phases [47] or refined grains [46] of duplex stainless steel could improve the chromium diffusion and promote the formation of compact passive film. This may involve the relationship between the galvanic effect and the geometry of the phases or grains. The more refinement the grains or phases, the more significant the galvanic effect between α and γ, and then the more significant the modification on the passive film. It gives us a clue that further refining α/γ size would greatly enhance the corrosion resistance of 2205 DSS. We will present such work shortly afterward.

4. Conclusions

The interaction between α and γ in DSS 2205 was investigated by combination of selective dissolution technique, conventional electrochemical measurements and localized electrochemical measurements. The results indicated that the interaction between α and γ in 2205 DSS favors the enhancement of the passive film. Galvanic effect between α and γ phases cannot deteriorate local corrosion. Under the galvanic effect, the diffusion of dissolved passive cations would be promoted in a short distance between α and γ zones, leading to modifications of chemical composition and semiconductive property of the passive film and therefore the enhancement of the corrosion resistance of DSS 2205. This indicates that further refining α and γ phases would markedly enhance the passive film on DSS 2205.

Acknowledgements

The authors acknowledge the support of the National Key Research and Development Program of China (No. 2016YFB0300604), the National Natural Science Foundation of China (No. 51671028).

References

[1] M. Conradi, P.M. Schön, A. Kocijan, M. Jenko, G.J. Vancso, Mater. Chem. Phys. 130 (2011) 708–713.
[2] H. Luo, C.F. Dong, K. Xiao, X.G. Li, Appl. Surf. Sci. 258 (2011) 631–639.
[3] N. Ebrahimi, M.H. Moayed, A. Davoodi, Corros. Sci. 53 (2011) 1278–1287.
[4] D.N. Zou, Y. Han, W. Zhang, G.W. Fan, J. Iron Steel Res. Int. 17 (2010) 67–72.
[5] M. Femenia, J. Pan, C. Leygraf, J. Electrochem. Soc. 151 (2004) 581–585.
[6] N. Sathirachinda, R. Pettersson, J. Pan, Corros. Sci. 51 (2009) 1850–1860.
[7] T. Souier, F. Martin, C. Bataillon, J. Cousty, Appl. Surf. Sci. 256 (2010) 2434–2439.
[8] A. Davoodi, M. Pakshir, M. Babaiee, G.R. Ebrahimi, Corros. Sci. 53 (2011) 399–408.
[9] X. Cheng, Z. Feng, C. Li, C. Dong, X. Li, Electrochim. Acta 56 (2011) 5860–5865.
[10] C.O.A. Olsson, Corros. Sci. 37 (1995) 467–479.
[11] I. Lo, Y. Fu, C. Lin, W. Tsai, Corros. Sci. 48 (2006) 696–708.
[12] W. Tsai, J. Chen, Corros. Sci. 49 (2007) 3659–3668.
[13] Y. Wang, X. Cheng, X. Li, Electrochem. Commun. 57 (2015) 56–60.
[14] M. Mouanga, M. Puiggali, O. Devos, Electrochim. Acta 106 (2013) 82–90.
[15] C. Dong, A. Fu, X. Li, Y. Cheng, Electrochim. Acta 54 (2008) 628–633.
[16] A.M. Simoes, A.C. Bastos, Corros. Sci. 49 (2007) 726–739.
[17] X. Cheng, X. Li, C. Dong, K. Xiao, Mater. Corros. 62 (2011) 1106–1110.
[18] J.B. Lee, Mater. Chem. Phys. 99 (2006) 224–234.
[19] S. Haupt, H.H. Strehblow, Corros. Sci. 37 (1995) 43–54.
[20] H. Jang, H. Kwon, J. Electroanal. Chem. 590 (2006) 120–125.
[21] C.A. Melendres, M. Pankuch, J. Electroanal. Chem. 333 (1992) 103–113.
[22] M. Urquidi-Macdonald, S. Real, D.D. Macdonald, J. Electrochem. Soc. 133 (1986) 2018–2024.
[23] H. Shin, F. Mansfeld, Corros. Sci. 28 (1988) 933–938.
[24] M. Urquidi-Macdonald, S. Real, D.D. Macdonald, Electrochim. Acta 35 (1990) 1559–1566.
[25] R. Jiang, Y. Wang, X. Wen, C. Chen, J. Zhao, Appl. Surf. Sci. 412 (2017) 214–222.
[26] Z.Y. Cui, L.W. Wang, H.T. Ni, W.K. Hao, X.G. Li, Corros. Sci. 118 (2017) 31–48.
[27] C. Boissy, B. Ter-Ovanessian, N. Mary, B. Normand, Electrochim. Acta 174 (2015) 430–437.
[28] A. Zaban, A. Meier, B.A. Gregg, J. Phys. Chem. B 101 (1997) 7985–7990.
[29] J. Lv, H. Luo, T. Liang, Mater. Res. Bull. 83 (2016) 148–154.
[30] F. Mohammadi, T. Nickchi, M.M. Attar, A. Alfantazi, Electrochim. Acta 56 (2011) 8727–8733.
[31] G.J. Brug, A.L.G. Eeden, M.S. Rehbach, J.H. Sluyters, J. Electroanal. Chem. 176 (1984) 275–295.
[32] M. Mouanga, M. Puiggali, B. Tribollet, V. Vivier, N. Pébère, Electrochemi. Acta 88 (2013) 6–14.
[33] Y. Zhou, X. Peng, F. Wang, Scr. Mater. 50 (2004) 1429–1433.
[34] D.D. Macdonald, Electrochim. Acta 56 (2011) 1761–1772.
[35] D.D. Macdonald, Pure Appl. Chem. 71 (1999) 951–978.
[36] D.D. Macdonald, J. Electrochem. Soc. 139 (1992) 3434–3449.
[37] D.A. Shirley, Phys. Rev. B 12 (1972) 4709–4714.
[38] D. Briggs, Handbook of X-ray Photoelectron Spectroscopy, Perkin-Elmer Corp., Minnesota, 1979.
[39] V. Vignal, H. Zhang, O. Delrue, O. Heintz, I. Popa, J. Peultier, Corros. Sci. 53 (2011) 894–903.
[40] I. Betova, M. Bojinov, V. Karastoyanov, P. Kinnunen, T. Saario, Electrochim. Acta 55 (2010) 6163–6173.
[41] H. Luo, X.Z. Wang, C.F. Dong, K. Xiao, X.G. Li, Corros. Sci. 124 (2017) 178–192.
[42] Y. Fu, X. Wu, E.-H. Han, W. Ke, K. Yang, Z. Jiang, Electrochim. Acta 54 (2009) 1618–1629.
[43] C. Clayton, Y. Lu, J. Electrochem. Soc. 133 (1986) 2465–2473.
[44] N. Padhy, R. Paul, U.K. Mudali, B. Raj, Appl. Surf. Sci. 257 (2011) 5088–5097.
[45] G.L. Song, Corros. Sci. 47 (2005) 1953–1987.
[46] J.L. Lv, T.X. Liang, C. Wang, L.M. Dong, Mater. Sci. Eng. C 62 (2016) 558–563.
[47] M. Atif Makhdoom, A. Ahmad, M. Kamran, K. Abid, W. Haider, Surf. Interfaces 9 (2017) 189–195.